Food and Chemical Toxicology 123 (2019) 492–500

Contents lists available at ScienceDirect

Food and Chemical Toxicology

journal homepage: www.elsevier.com/locate/foodchemtox

Plumbagin from a tropical pitcher plant (*Nepenthes alata* Blanco) induces apoptotic cell death via a p53-dependent pathway in MCF-7 human breast cancer cells

Umasankar De[a], Ji Yeon Son[a], Yukyoung Jeon[a], Song-Yi Ha[a], Yu Jin Park[a], Sungpil Yoon[a], Ki-Tae Ha[b], Wahn Soo Choi[c], Byung Mu Lee[a], In Su Kim[a], Jong Hwan Kwak[a,*], Hyung Sik Kim[a,*]

[a] School of Pharmacy, Sungkyunkwan University, Suwon, 16419, Republic of Korea
[b] School of Korean Medicine and Healthy Aging Korean Medicine Research Center, Pusan National University, Yangsan, 50612, Republic of Korea
[c] School of Medicine, Konkuk University, Chungju, 27478, Republic of Korea

ARTICLE INFO

Keywords:
Anticancer
Nepenthes alata
Plumbagin
Apoptosis
p53
Reactive oxygen species

ABSTRACT

Plumbagin (5-hydroxy-2-methyl-1,4-naphthaquinone) has displayed antitumor activity *in vitro* and in animal models; however, the underlying molecular mechanisms have not been fully explored. The aim of this study was to investigate the anticancer effects of plumbagin isolated from *Nepenthes alata* against MCF-7 breast cancer cells. We examined the cytotoxicity, cell cycle regulation, apoptotic cell death, and generation of intracellular reactive oxygen species (ROS) in MCF-7 cells. Plumbagin exhibited potent cytotoxicity in MCF-7 cells (wild-type p53) compared to that in SK-OV-3 (null-type) human epithelial ovarian cancer cells. Specifically, plumbagin upregulated the expression of $p21^{CIP1/WAF1}$ in MCF-7 cells, causing cell cycle arrest in the G2/M phase through inhibition of cyclin B1 levels. Plumbagin also significantly increased the ratio of Bax/Bcl-2 and release of cytochrome c, resulting in apoptotic cell death in MCF-7 cells. Furthermore, plumbagin dramatically increased the intracellular ROS level, whereas pretreatment with the ROS scavenger N-acetyl cysteine protected against plumbagin-induced cytotoxicity, suggesting that ROS formation plays a pivotal role in antitumor activity in MCF-7 cells. In mice bearing MCF-7 cell xenografts, plumbagin significantly reduced tumor growth and weight without apparent side effects. We therefore concluded that plumbagin exerts anticancer activity against MCF-7 cells through the generation of intracellular ROS, resulting in the induction of apoptosis via a p53-dependent pathway. This study thus identifies a new anticancer mechanism of plumbagin against p53-dependent breast cancer cells and suggests a novel strategy for overcoming of breast cancer therapy.

1. Introduction

Nepenthes constitutes a genus of carnivorous plants popularly known as tropical pitcher plants in the monotypic family Nepenthaceae. The genus comprises 70 species of climbing or scrambling, terrestrial, or epiphytic dioecious carnivorous perennial shrubs or semi-woody herbs distributed throughout Madagascar, the Seychelles, and tropical Asia to Australia (northern Queensland). In particular, *Nepenthes alata* Blanco grows naturally in the Philippines, Malaysia, Borneo, and Sumatra and represents one of the most popular *Nepenthes* in cultivation worldwide (Cannon et al., 1980; Huxley et al., 1999). However, although several studies have reported information regarding the plant physiology and carnivorous syndrome of *N. alata* (Bauer and Federle, 2009; Hafeez et al., 2013; Mithöfer, 2011), this species has not been pharmacologically investigated.

Plumbagin (5-hydroxy-2-methyl-1,4-naphthoquinone) was initially isolated from the roots of *Plumbago zeylanica*, *P. rasea*, and *P. europoea* (Padhye et al., 2012) and has also been identified in several *Nepenthes* plants (Schlauer et al., 2005). It has been reported that plumbagin exhibits antimicrobial, anti-inflammatory, and anticancer activities (Buch

Abbreviations: ATCC, American Type Culture Collection; AO, acridine orange; DMEM, Dulbecco's modified Eagle's medium; DMSO, dimethylsulfoxide; DCF-DA, 2′,7′-dichlorofluorescin diacetate; DPBS, Dulbecco's Phosphate Buffered Saline; ECL, enhanced chemiluminescence; EtBr, ethidium bromide; FBS, fetal bovine serum; MDM2, mouse double minute 2 homolog; NAC, N-acetyl cysteine; RT-PCR, reverse transcription polymerase chain reaction; PCNA, proliferating cell nuclear antigen; PARP, poly-ADP-ribose polymerase; PVDF, polyvinylidene difluoride; PI, propidium iodine; ROS, reactive oxygen species; TUNEL, terminal deoxynuclotidyl transferase dUTP nick end labeling

* Corresponding authors. School of Pharmacy, Sungkyunkwan University, 2066, Seobu-ro, Jangan-gu, Suwon, Gyeonggi-do, 16419, Republic of Korea.
E-mail addresses: jhkwak@skku.edu (J.H. Kwak), hkims@skku.edu (H.S. Kim).

https://doi.org/10.1016/j.fct.2018.11.040
Received 29 May 2018; Received in revised form 14 November 2018; Accepted 16 November 2018
Available online 17 November 2018
0278-6915/

et al., 2013; Padhye et al., 2012). Numerous studies have investigated the anticancer effects of plumbagin against various human breast, ovarian, lung, and prostate cancer cells (Aziz et al., 2008; Gowda et al., 2017; Kawiak et al., 2017; Manu et al., 2011; Nair et al., 2016; Qiao et al., 2016; Sinha et al., 2013; Thasni et al., 2013; Wei et al., 2017), resulting in this compound being considered as a candidate for clinical application in patients with cancer. The molecular mechanisms of the anticancer activities of plumbagin include changes in various signaling pathways such as those involved in cancer cell proliferation, apoptosis, invasion, and metastasis through the regulation of major signaling molecules depending on cancer cell type or origin (Gowda et al., 2017; Padhye et al., 2012; Wei et al., 2017). Experimental evidence also suggests that the tumor suppressor p53 is associated with the anticancer mechanisms of plumbagin (Pan et al., 2015; Zhang et al., 2016). Activated p53, one of the best-known tumor suppressors, represents a promising target for the inhibition of tumor growth (Girardini et al., 2014; Wang et al., 2015). Notably, however, in previous studies the cytotoxic mechanisms of plumbagin were closely related to p53 activation in certain cancer cell lines (Sagar et al., 2014; Zhang et al., 2016), whereas p53-independent pathways were involved in others (Manu et al., 2011; Pan et al., 2015). However, the effects of plumbagin on breast cancer and the underlying molecular mechanisms remain unclear.

In this study, plumbagin was isolated from *N. alata* as a compound exhibiting high cytotoxicity against MCF-7 (p53-wild-type human breast cancer) cells, especially compared to that in SK-OV-3 (p53-null human epithelial ovarian cancer) and normal cell lines. In our investigation, we mainly focused on plumbagin-mediated anticancer activity against MCF-7 cells in a p53-dependent manner. In addition, we further investigated the cell death mechanisms of plumbagin and its *in vivo* efficacy using xenograft models.

2. Materials and methods

2.1. Plant material

Whole plants of *N. alata* were purchased from the Yangjae Flower Market Center in Seoul, Korea, in September 2013. A voucher specimen (SKKU-Ph-13-008) was deposited in the School of Pharmacy, Sungkyunkwan University.

2.2. Extraction and isolation of plumbagin

Roots of *N. alata* were cut into small pieces and lyophilized at −50 °C for 30 h. The dried specimen (363 g) was extracted twice with methanol (MeOH) at room temperature and once with MeOH at 60 °C. All extracts were combined and the solvent was removed under reduced pressure to yield MeOH extract (MeOH Ex., 37.55 g). The MeOH extract was suspended in distilled water (400 mL) and then sequentially partitioned with dichloromethane, ethyl acetate, and *n*-butanol. Each of the solvent fractions was evaporated under reduced pressure to give dichloromethane (CH_2Cl_2 fr., 6.31 g), ethyl acetate (EtOAc fr., 5.84 g), *n*-butanol (*n*-BuOH fr., 11.14 g), and water (H_2O fr., 15.35 g) fractions. Among these, the dichloromethane fraction, which showed the strongest cytotoxicity, was subjected to activity-guided chromatographic separation. The CH_2Cl_2 fraction was further fractionated on a silica gel column using stepwise elution with hexane-EtOAc (10:1, 3:1, and 1:2) and CH_2Cl_2-MeOH (5:1) to give 10 subfractions (MC-1 to MC-10). Fraction MC-2 was rechromatographed over a silica gel column (hexane-CH_2Cl_2, 2:1), and one of the resulting fractions was applied to a reversed phase (RP)-C_{18} column (85% MeOH in water) to obtain compound **1** (33.5 mg). Compound **1** was subjected to RP-C_{18} high performance liquid chromatography (HPLC) using a gradient elution to determine the purity. The eluent consisted of MeOH (A) and water (B), and the gradient profile was as follows: 0–5 min, isocratic 50% A in B; 5–20 min, linear change from 50% to 80% A in B; 20–25 min, isocratic 80% A in B; 25–30 min, linear change from 80% to 100% A in B. The flow rate and injection volume were 1 mL/min and 20 μL, respectively. Column temperature was maintained at 35 °C, and ultraviolet absorption was measured at a wavelength of 254 nm.

2.3. General experimental procedures

Nuclear magnetic resonance experiments were performed on a Varian Unity INOVA 500 spectrometer (Palo Alto, CA, USA) with the usual pulse sequence, and chemical shifts (δ) are reported in parts per million, referenced to the solvent used. A Hewlett-Packard HP 6890 series Gas Chromatography (GC) system coupled with a Hewlett-Packard 5973 mass selective detector (Palo Alto, CA, USA) was used to obtain GC/Electrone Ionization Mass Spectrometry (EIMS) spectra. Column chromatography was performed on silica gel 60 (230–400 mesh, Merck, Darmstadt, Germany) and LiChroprep RP-18 (40–63 μm, Merck). Thin-layer chromatography was carried out on pre-coated silica gel 60 F_{254} plates (Merck) and RP-18 F_{254s} plates (Merck). HPLC analysis was performed with a Knauer Smartline system (Manager 5000, two Pump 1000, and UV Detector 2500; Berlin, Germany) equipped with a phenomenex 5 μm C18 100A Kinetex column (150 × 4.6 mm; Phenomenex, Torrance, CA, USA) using gradient elution.

2.4. Chemicals and reagents

Cell culture medium, fetal bovine serum (FBS), epidermal growth factor, and supplements were obtained from Gibco Invitrogen Corporation (Carlsbad, CA, USA). Primary antibodies against poly-ADP-ribose polymerase (PARP), Bax, Bcl-2, p53, phospho-p53, p21, cyclin A, cyclin B1, mouse double minute 2 homolog (MDM2), and cytochrome c along with horseradish peroxidase-conjugated secondary antibody were purchased from Santa Cruz Biotechnology (Dallas, TX, USA). All other chemicals were purchased from Sigma-Aldrich (St. Louis, MO, USA). Plumbagin was dissolved in dimethyl sulfoxide (DMSO) and stored at −20 °C until use. The stock solution was diluted to appropriate concentrations with culture medium containing 1% FBS. The final concentration of DMSO was less than 0.1% (v/v) and was also present in the corresponding controls.

2.5. Cell culture

The MCF-7 (human breast cancer) and SK-OV-3 (human epithelial ovarian cancer) cell lines were purchased from the American Type Culture Collection (ATCC, Manassas, VA, USA). Cells were grown in Dulbecco's modified Eagle's medium (Gibco, Rockville, MD, USA) containing 10% heat-inactivated FBS and 1 unit/mL penicillin/streptomycin (Gibco). The MCF-10A cell line (normal breast cells) was purchased from the ATCC and maintained in complete growth medium consisting of a 1:1 mixture of Dulbecco's modified Eagle's medium and Ham's F12 medium supplemented with 5% FBS, 20 ng/mL epidermal growth factor (EGF), 10 μg/mL insulin, 500 ng/mL hydrocortisone, and 1 unit/mL penicillin/streptomycin. Cells were maintained as monolayers in a humidified atmosphere containing 5% CO_2 at 37 °C, and the culture medium was replaced every 2 days.

2.6. Cytotoxicity assay

Cytotoxicity was determined using 3-(4,5-dimethylthiazol-2-yl)-2,5-diphenyl-tetrazolium bromide (MTT, Sigma-Aldrich). Cells were seeded in 96-well culture plates at a density of 2×10^3 cells/mL in complete growth medium at 37 °C in a humidified incubator. After incubation for 24 h, cells were exposed to plumbagin at various concentrations and cultured for a further 24 h and 48 h. At the end of treatment, 15 μL of MTT reagent (5 mg/mL) was added to each well and incubated for 3 h at 37 °C in the dark. The supernatant was aspirated, and formazan crystals were dissolved in 150 μL DMSO at 37 °C for 15 min with gentle

agitation. The absorbance per well was measured at 540 nm using the VERSA Max microplate reader (Molecular Devices Corp., Sunnyvale, CA, USA). Data were analyzed from three independent experiments and normalized to the absorbance of wells containing medium only (0%) and untreated cells (100%). IC_{50} values were calculated from sigmoidal dose-response curves using *SigmaPlot* 10.0 software (Systat Software, Chicago, IL, USA).

2.7. Immunofluorescence assay

The MCF-7 cells were seeded into 35 mm cover-glass bottom dishes at density of 1×10^5 cells. After overnight incubation with plumbagin cells were fixed with 100% chilled methanol at room temperature for 10 min and then permeabilized with 0.2% Triton X-100 in PBS for 10 min. Followed by cells were blocked with 1% BSA, 0.3 M glycine in PBST (PBS +0.1% Tween 20) blocking buffer for 30 min to prevent nonspecific antibody binding and later incubated diluted primary anti-antibody (p-p53 and MDM2 with 1: 50 ratio) in blocking buffer overnight at 4 °C. After incubation cells were washed and then incubated with secondary antibody (AlexaFluro goat anti-rabbit IgG, 1:500; Abcam; USA) at room temperature. Finally cells were stain with DAPI for 30 min and image were analyzed using confocal laser fluorescence microscopy and ZEN 2011 software (Zeiss, Oberkochen, Germany).

2.8. Cell cycle analysis

Cultured cells were treated with various concentrations of plumbagin for 48 h. Harvested cells (5×10^5) were washed with PBS containing 1% BSA, fixed in chilled 95% ethanol, stained with propidium iodide (PI) staining solution (10 μg/mL PI and 100 μg/mL RNase in PBS), and incubated in the dark for 30 min at room temperature. Data acquisition and analysis were carried out using a Guava EasyCyte Plus flow cytometer (Merck Millipore, Billerica, MA, USA).

2.9. Annexin V-FITC binding assay

The Annexin V-FITC binding assay was performed using the Annexin V-FITC detection kit I (BD Biosciences, San Diego, CA, USA) according to the manufacturer's instructions. The cells were treated with plumbagin for 24 h. The total number of cells was counted after trypsinization and cells were washed twice with cold PBS. The cell pellet was resuspended with 100 μM binding buffer at a density of 1×10^4 cells/mL and incubated with 5 μL of FITC-conjugated Annexin V and 5 μL of PI for 15 min at room temperature in the dark. After addition of 400 μL of 1 × binding buffer to each tube, the samples were immediately analyzed using a Guava EasyCyte Plus flow cytometer (Merk Millipore).

2.10. Western blot analysis

After treatment with 5 μM plumbagin for various times, cells were harvested by trypsinization and washed twice with cold PBS. For isolation of total protein, cells were suspended in PRO-PREP™ protein extract solution (iNtRON, Seongnam, Korea), and protein concentration was measured using a protein assay kit (Bio-Rad, Hercules, CA, USA) according to the manufacturer's instructions. Cell extract containing 20 μg protein was separated by electrophoresis on a 6–15% sodium dodecyl sulphate-polyacrylamide gel and transferred to a polyvinylidene difluoride membrane (Millipore). The membrane was incubated for 1 h in TNA (10 mM Tris-Cl, pH 7.6, 100 mM NaCl, and 0.5% Tween 20) buffer containing 5% skim milk and incubated with primary antibodies at 4 °C overnight. The membrane was washed for 1 h with TNA buffer and then incubated with horseradish peroxidase-conjugated anti-mouse or anti-rabbit antibodies (1:10000, Santa Cruz) for 30 min at room temperature. The blots were developed using an enhanced chemiluminescence (ECL)-plus kit (Amersham Biosciences, Amersham, Buckinghamshire, UK).

2.11. Acridine orange/ethidium bromide double staining

MCF-7 cells were cultured in a 35-mm dish and treated with plumbagin for 24 h. Cells were stained with acridine orange (50 mg/mL) or ethidium bromide (50 mg/mL) by incubation for 15 min and then washed three times with Dulbecco's PBS to remove extracellular dye. Images were analyzed by confocal laser fluorescence microscopy using a ZEN 2011 laser scanning microscope software (Zeiss, Oberkochen, Germany).

2.12. DAPI staining

Seed cells were treated with plumbagin for 24 h, after that we perform cell fixation using 4% formaldehyde than stain with DAPI for 20 min at room temperature. After washing with PBS, image was taken by confocal laser fluorescence microscopy using ZEN 2011 laser scanning microscope software (Zeiss, Oberkochen, Germany).

2.13. Measurement of reactive oxygen species (ROS) generation

The formation of intracellular ROS was assayed by the fluorescence emission of 2′,7′-dichlorofluorescin diacetate (DCFDA), which penetrates into the cytoplasm of the cell where it is hydrolyzed by intracellular esterase and oxidized by ROS to form DCF. Briefly, cells (1×10^5) were seeded into 35-mm glass bottom dishes and treated with plumbagin for 24 h. After washing with PBS, cells were incubated with 10 μM DCFDA at 37 °C for 10 min. Images were captured by fluorescence microscopy (Zeiss Axiovert 200, Carl Zeiss, Thornwood, NY, USA). After cells were detached and centrifuged, cell pellets were suspended in phenol red-free Dulbecco's modified Eagle's medium. The fluorescence intensity of each cell suspension (5000 cells/sample) was quantified using the Guava Easy Cyte Plus flow cytometer system at 495/529 nm.

2.14. In vivo xenograft model

Six-week-old female nude mice weighing approximately 20 g (BALB-c nu/nu, Japan SLC, Inc., Hamamatsu, Shizuoka, Japan) were housed under controlled temperature (22 ± 2 °C) and a 12-h light/dark cycle in filtered-air laminar-flow cabinets and handled using aseptic procedures. The institutional animal care committee of Sungkyunkwan University approved the experimental procedure (2017-15-034). MCF-7 cells (10×10^6 cells/0.1 mL) in serum-free medium containing 50% Matrigel (BD Biosciences, 354234) were injected subcutaneously. Prior to drug administration, mice were randomly assigned into two groups (n = 5 per group): the first group of mice was treated with plumbagin intraperitoneally (i.p.) at 2 mg/kg body weight in 0.2 mL PBS, 5 days per week for 45 days, whereas the second group (control mice) was treated in the same manner with vehicle (0.2 mL PBS). Tumor volume (V) was calculated using the standard formula, V (mm^3) = 0.52 ($ab2$), where a is the length and b is the width of the tumor. Body weights were recorded prior to dosing and at termination. On day 45, the mice were sacrificed by carbon dioxide asphyxiation.

2.15. Statistical analysis

The data are expressed as the means ± SD of at least three independent experiments. Statistical analysis was performed using one-way analysis of variance (ANOVA) followed by Bonferroni's multiple comparison tests. *p-value < 0.05 and **p-value < 0.01 were considered statistically significant.

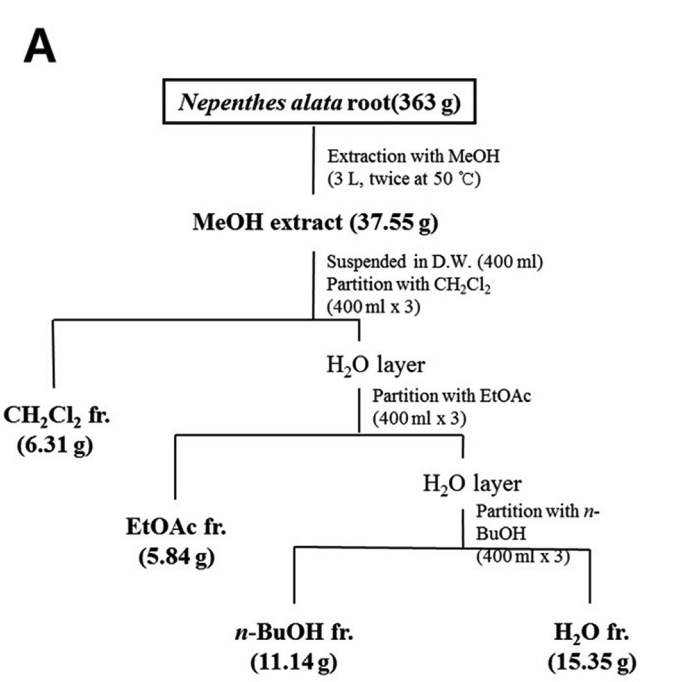

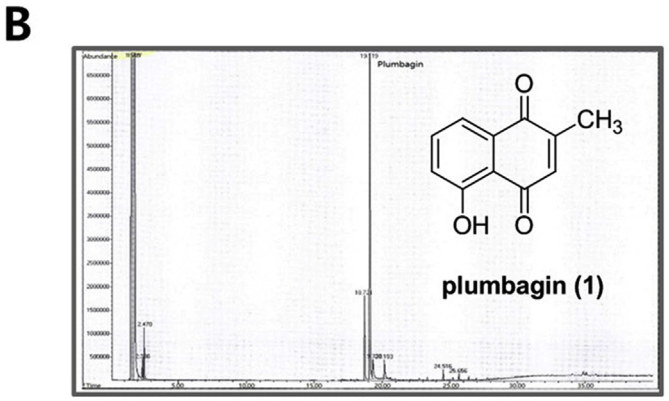

C

IC_{50} value on MCF-7 cells

Extract and fractions	24 h (μg/mL)	48 h (μg/mL)
MeOH ex.	99.78	95.88
CH_2Cl_2 fr.	36.60	34.55
EtOAc fr.	90.02	85.36
n-BuOH fr.	61.13	47.98
H_2O fr.	>100	>100

Fig. 1. Cytotoxicity of the extract and solvent fractions from *Nepenthes alata* root against human cancer cell lines. (A) Extraction and fractionation scheme of *N. alata* root. (B) Structure of plumbagin (1) and GC chromatogram of the CH_2Cl_2 fraction from the MeOH extract of *N. alata* root. (C) Cytotoxic effect of the extract and solvent fractions from *N. alata* root against MCF-7 cells.

3. Results

3.1. Cytotoxicity of the extract and solvent fractions from Nepenthes alata root against MCF-7 cells

The MeOH extract of *Nepenthes alata* roots was solvent partitioned consecutively with CH_2Cl_2, EtOAc, and *n*-BuOH (Fig. 1A) and the cytotoxicity of each level against MCF-7 cells was determined. The CH_2Cl_2 fraction, which showed significant MCF-7 cell cytotoxicity (Fig. 1C; IC_{50} values: 36.60 μg/mL at 24 h and 34.55 μg/mL at 48 h), was subjected to column chromatographic separation and purification. Compound **1** (Fig. 1B) was isolated from the CH_2Cl_2 fraction by silica gel and RP-C_{18} column chromatography and identified as plumbagin by comparison of its spectroscopic data with literature values (Buch et al., 2013; Cannon et al., 1980; Rischer et al., 2002). Plumbagin has been previously reported from *Nepenthes* plants and also identified as a mixture from *N. alata* (Mithofer, 2011; Raj et al., 2011; Rischer et al., 2002; Schlauer et al., 2005); however, herein it was isolated for the first time from *N. alata.* Compound **1** was determined to have > 98% purity by HPLC analysis.

3.2. Plumbagin exhibits higher cytotoxicity in p53 wild-type MCF-7 cells compared with p53-null SK-OV-3 cells

The anticancer effect of plumbagin against different cancer or normal cell lines was evaluated by MTT assay. Multiple concentrations of plumbagin were used and effective doses were calculated from dose-response curves. Results of the cytotoxicity evaluation against MCF-7 and SK-OV-3 cells are shown in Fig. 2. Plumbagin exhibited potent cytotoxicity against MCF-7 cells, achieving an IC_{50} value of 3.5 μM at 48 h treatment. In contrast, plumbagin exhibited moderate cytotoxic effect against the SK-OV-3 cell line with an IC_{50} value of 13.1 μM at 48 h treatment. We also measured the cytotoxicity of plumbagin against non-cancerous MCF-10A breast cells. Although plumbagin exhibited moderate cytotoxicity against MCF-10A cells in a concentration-dependent manner, comparison of the results indicated that MCF 7 cells exhibited two-fold greater sensitivity to plumbagin than MCF-10A cells (Figs. 2B and 2F).

As p53 activation is involved in anticancer drug activity (Wang et al., 2015; Zhang et al., 2016), we examined whether the anticancer activity of plumbagin correlated with expression of p53 in MCF-7 breast cancer cells, which express wild-type p53. As shown in Fig. 3A, levels of both p53 and its activated form phosphorylated (phospho)-p53 were increased after 24 h of plumbagin treatment. Specifically, p53 protein level increased initially and then activated phospho-p53 level increased further in a time-dependent manner. In SK-OV-3 cells, plumbagin treatment did not change the level of either p53 protein or phospho-p53, as expected for p53-null cells (Fig. 3B), suggesting that plumbagin decreased MDM2 protein levels independent of p53. Immunocytochemistry indicated that phospho-p53 was translocated into the nucleus, wherein the transcription of target genes might be activated (Fig. 3C). We therefore evaluated whether the nuclear translocation of p53 might explain any of the presumably MDM2-mediated changes in MCF-7 cells. Plumbagin treatment dramatically reduced the MDM2 expression in MCF-7 cells (Fig. 3D), suggesting that activation of p53 was closely associated with reduced MDM2 levels in this cell line.

3.3. Plumbagin stimulates G2/M arrest via reduced cyclin B1 in MCF-7 cells

We further investigated the mechanisms by which plumbagin decreased the viability of MCF-7 cancer cells. We examined time-dependent changes in important cell cycle proteins (Kim et al., 2014, 2015) to determine which proteins show early changes and the duration of such effects. As shown in Fig. 4A, the level of cyclin B1 was markedly decreased at an early time point, suggesting that G2/M-related cyclin proteins were affected. However, cyclin A expression was not changed (Fig. 4A). Notably, expression of p21 was increased by plumbagin at a late time point (Fig. 4A), which suggested that plumbagin arrests the cell cycle through p53-mediated transcriptional regulation of the downstream p21 protein in MCF-7 cells. To obtain detailed results of

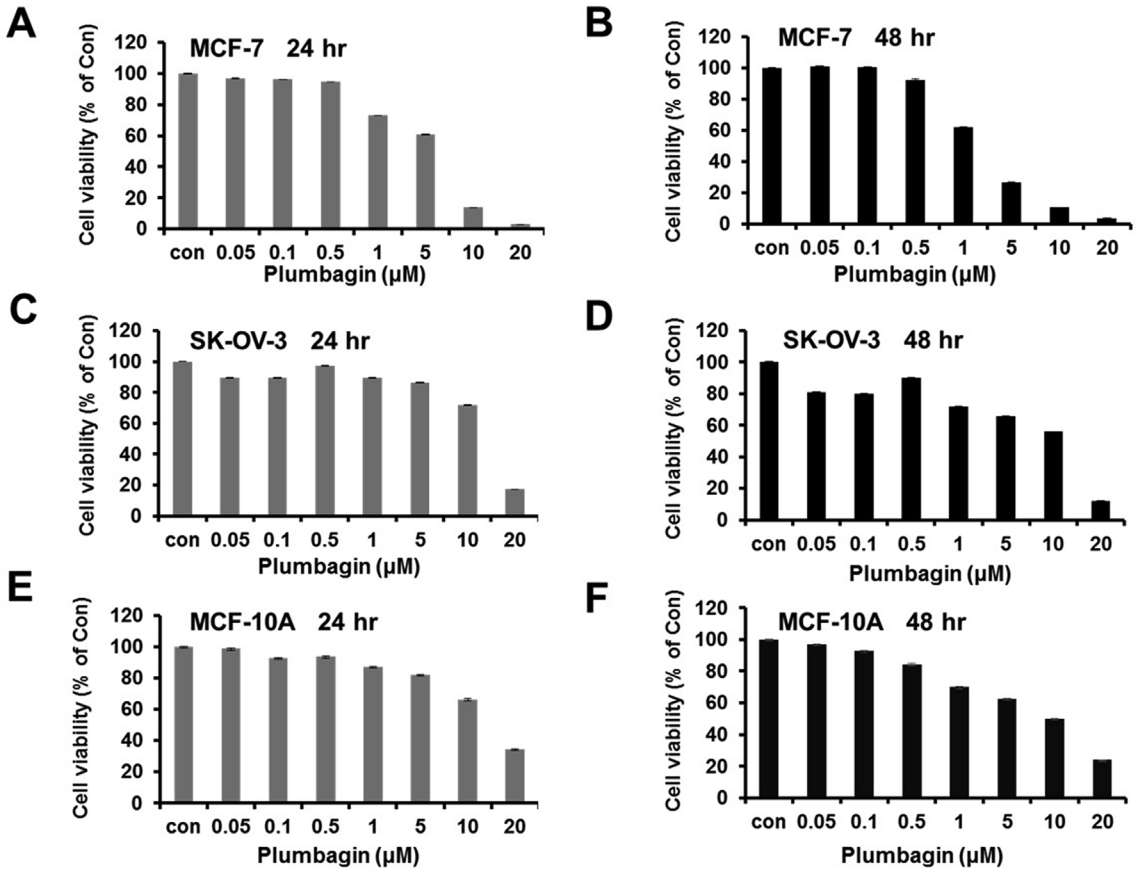

Fig. 2. Cytotoxicity of plumbagin against MCF-7 (A), SK-OV-3 (B), and MCF-10A (C) cells. Cells were treated with plumbagin at various concentrations (0.05–20 μM) and cytotoxicity was measured by MTT assay. Each value represents the mean ± SD from three independent experiments.

cell cycle regulation, we performed flow cytometry analysis with the indicated concentrations of plumbagin (2 or 5 μM) in MCF-7 cells. Plumbagin predominantly induced the G2/M phase arrest (Fig. 4B). The low concentration of 2 μM plumbagin increased G2/M phase arrest as efficiently as 5 μM, suggesting that the low concentration is sufficient to produce maximum G2/M arrest. Collectively, our data demonstrated that plumbagin induced G2/M phase arrest through both reduced cyclin B1 and increased p21 level.

3.4. Plumbagin induces apoptosis in MCF-7 cells

As shown in Fig. 4B, treatment of MCF-7 cells with a high concentration (5 μM) of plumbagin led to increase in the sub-G1 cell population. To elucidate the apoptotic pathway underlying the cytotoxic effect of plumbagin, expression levels of apoptosis-related proteins were measured by western blot analysis. Plumbagin increased the levels of cleaved PARP and Bax, whereas that of the anti-apoptotic protein

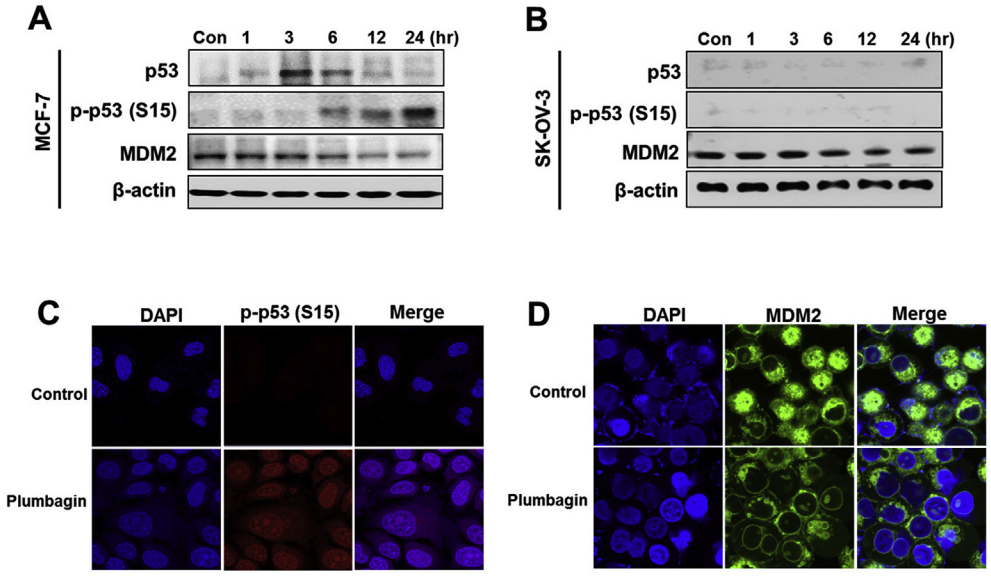

Fig. 3. Plumbagin is more effective in p53 wild-type MCF-7 compared with p53-null SK-OV-3 cells. MCF-7 (A) and SK-OV-3 (B) cells were treated with 5 μM plumbagin at various times and then western blot analysis was performed with antibodies to p53, phospho-p53, MDM2, and β-actin (as a loading control). (C and D) Immunostaining of MCF-7 cells for phospho-p53 and MDM2 in MCF-7 cells. The cells were treated with plumbagin at the indicated concentration for 24 h and stained with primary antibody against phospho-p53 and MDM2.

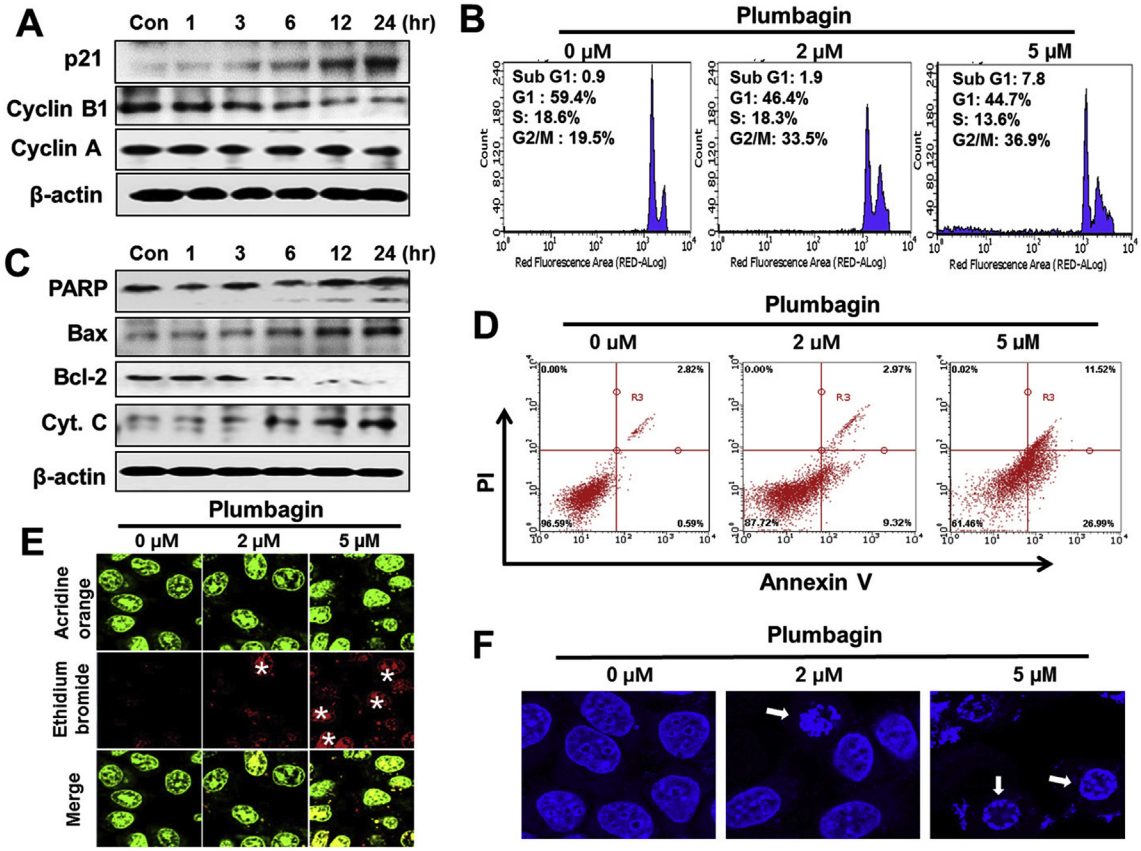

Fig. 4. Plumbagin increases apoptotic cell death via G2-arrest with dose-dependence in MCF-7 cells. (A) MCF-7 cells were treated with plumbagin (5 μM) and then western blot analysis was performed with antibodies against p21, cyclin A, cyclin B1, and β-actin (as a loading control). (B) The cultured cells were treated with various concentrations of plumbagin for 24 h and total numbers of cells were analyzed using flow cytometry. (C) To confirm apoptosis, MCF-7 cells were treated with plumbagin (5 μM) and then western blot analysis was performed with antibodies to PARP, Bax, Bcl-2, cytochrome c, and β-actin (as a loading control). (D) To perform Annexin V/PI double staining, the cells were treated with plumbagin (0, 2, or 5 μM) for 24 h and then analyzed using the Guava EasyCyte Plus flow cytometer. (E) MCF-7 cell was treated with plumbagin (0, 2, or 5 μM) for 24 h. Acridine orange/ethidium bromide (AO/EtBr) staining was used to determine morphological changes. (F) MCF-7 cells were treated with plumbagin (0, 2, or 5 μM) for 24 h and apoptotic body formation (arrows) as an indicator of apoptosis was determined by DAPI staining followed by photographing cells under fluorescence microscopy as described in the Materials and Methods. White arrows show the characteristic morphological changes of apoptosis, including nuclear condensation and DNA fragmentation induced by plumbagin (2 or 5 μM) treatment. (For interpretation of the references to colour in this figure legend, the reader is referred to the Web version of this article.)

Bcl-2 was decreased (Fig. 4C). We further performed annexin V-FITC/PI double staining for a more detailed analysis of early or late apoptosis in MCF-7 cells. The percentage of early-stage apoptotic cells was greatly increased by treatment with 2 μM plumbagin, whereas 5 μM plumbagin largely increased the late-stage apoptotic cell population (Fig. 4D). EtBr/AO staining was also performed to evaluate the morphological changes in MCF-7 cells treated with plumbagin. The number of apoptotic cells significantly increased in a concentration-dependent manner after plumbagin treatment (Fig. 4E). To confirm our assumption that plumbagin-mediated apoptotic pathways contributed to the p53-related sensitization of MCF-7 cells, we also assessed the characteristic nuclear changes that differentiate apoptosis from necrosis. As shown in Fig. 4F, staining with DAPI, a nuclear stain that is observed as blue fluorescence when excited under a fluorescence microscope, revealed the changes associated with apoptosis in MCF-7 cells treated with plumbagin. In particular, the characteristic morphological changes by apoptosis such as chromatin condensation and nuclear fragmentation were clearly observed in the plumbagin-treated MCF-7 cells. These findings suggest that plumbagin induced apoptotic death of MCF-7 cells via traditional mitochondrial-related apoptotic pathways.

3.5. Plumbagin increases intracellular ROS generation

As the marked increase in apoptosis induced by plumbagin may have resulted from the generation of intracellular ROS, we measured intracellular ROS levels using the fluorescence emission of DCFDA upon hydrolysis to DCF by ROS. As shown in Fig. 5A and B, exposure of MCF-7 cells to hydrogen peroxide (50 μM) as a positive control significantly increased ROS production by approximately 4-fold compared to the untreated control. As expected, plumbagin substantially induced ROS generation in MCF-7 cells. In addition, plumbagin-treated MCF-7 cells exhibited a robust, dose-dependent increase in intracellular ROS production. As the level of ROS generation induced by plumbagin was higher in MCF-7 cells compared to that in other cells or by other drugs (data not shown), we assumed that the increased ROS generation by plumbagin could explain the relatively low IC_{50} in MCF-7 cells. ROS production was also measured with DCFDA using flow cytometry (Fig. 5C). We examined the effect of the free radical scavenger N-acetyl cysteine (NAC) on plumbagin-dependent ROS production in MCF-7 cells. Co-treatment with NAC resulted in almost complete inhibition of plumbagin-induced ROS production (Fig. 5D). We also determined the effects of NAC on plumbagin-induced cytotoxicity. As shown in Fig. 5E, almost complete suppression of plumbagin-induced cytotoxicity was observed upon exposure to plumbagin in the presence of NAC.

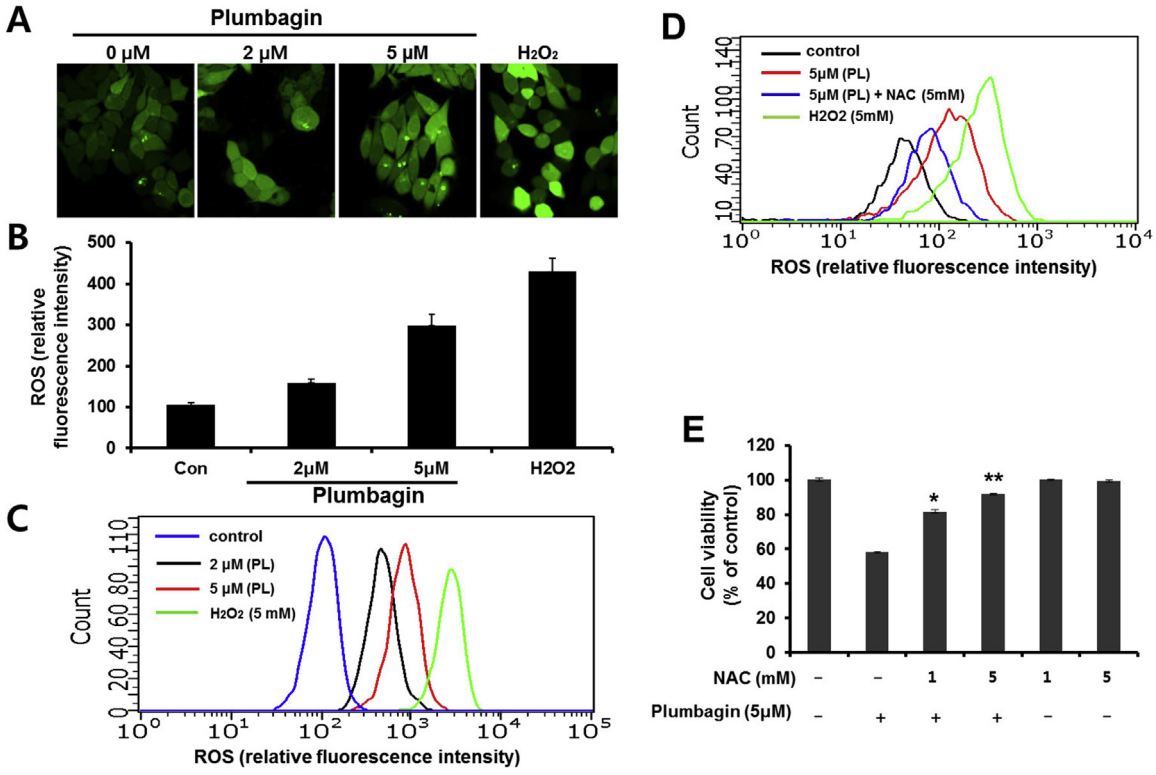

Fig. 5. Plumbagin-induced intracellular ROS generation in MCF-7 cells. MCF-7 cells were treated with the indicated concentrations of plumbagin or hydrogen peroxide (50 μM) for 12 h, and then cells were treated with fluorescence emission of DCFDA. (A) Fluorescence microscopy images showing the qualitative ROS generation by plumbagin in MCF-7 cells. (B) Bar histogram for the mean intensity of the DCF-related fluorescence expressed as fold-change of the untreated cells; data represent the means ± SD of three independent experiments. (C) Data indicating the quantification of the fluorescence intensity as carried out using a Guava EasyCyte plus Flow Cytometer. (D) N-acetyl cysteine (NAC) abolishes plumbagin-induced ROS accumulation in MCF-7 cells. ROS production was measured with DCFDA using flow cytometry. (E) Effect of NAC (ROS inhibitor) on plumbagin-induced MCF-7 cell cytotoxicity. Data shown are typical representatives of three independent experiments. *$p < 0.05$; **$p < 0.01$ were considered as significant.

3.6. Plumbagin reduces the growth of MCF-7 cell-based tumors in a xenograft model

To evaluate the antitumor effects of plumbagin *in vivo,* we used an MCF-7 tumor xenograft model developed with BALB/c nude mice. Plumbagin was injected at 2 mg/kg body weight for 45 days. Treatment with plumbagin markedly inhibited the increase in tumor volume compared to a vehicle-treated control group; the final tumor size in mice treated with plumbagin was approximately 75% lower than that in control mice. Plumbagin treatment also resulted in a significant decrease in tumor weight compared to control mice (Fig. 6A). During the days after plumbagin treatment, the tumor size increased very slowly, and the tumor volume was nearly the same as that in the initial 10 days (Fig. 6B). These data clearly indicated that plumbagin significantly inhibits the growth of MCF-7 cells *in vivo*. Additionally, regular monitoring of body weight in plumbagin-treated mice during the test period indicated no signs of unusual toxic effects (data not shown). To determine whether the p53-related apoptotic pathway was responsible for the antitumor effects of plumbagin in the *in vivo* model, we performed western blot analysis of apoptosis-related proteins. As shown in Fig. 6C, levels of p53 and the phospho-p53 increased in plumbagin-treated mice, similar to results of the *in vitro* study. In addition, the plumbagin-treated group showed markedly increased relative protein expression levels of cleaved PARP and Bax (Fig. 6D). Taken together, these results indicated that plumbagin induced p53-dependent apoptosis in the *in vivo* model via intrinsic pathways.

4. Discussion

Plumbagin was isolated from *N. alata* and the molecular mechanism of its anticancer activity was investigated using cancer cell lines with either p53 wild-type (MCF-7) or p53 null (SK-OV-3). Our data clearly demonstrated that plumbagin exhibited concentration- and time-dependent cytotoxicity against p53 wild-type MCF-7 cells.

Based on our findings on the levels of p53 and its activation, we concluded that p53 is an important factor in the sensitization of cancer cells to plumbagin. Therefore, we hypothesized that the anticancer effect of plumbagin is closely related to the p53-dependent signaling pathway, consistent with previous studies suggesting that plumbagin-induced cell cycle arrest is associated with p53 status (Tian et al., 2012; Zhang et al., 2016). In addition, we found that plumbagin also reduced MDM2 protein level in MCF-7 cells in a time-dependent manner. As MDM2 is an upstream negative regulator of p53 (Inoue and Fry, 2016), further analysis is required to clarify whether plumbagin-mediated downregulation of MDM2 levels correlates with or directly contributes to the p53 phosphorylation. In turn, the significant increase in p21 level after treatment with plumbagin suggested that activated form of p53 enters the nucleus to induce transactivation of p21, leading to cell cycle arrest in the G2/M phase by binding of the cyclin-cdk complex. The influence of plumbagin-mediated cell cycle patterns in MCF-7 cells requires further investigation. Indeed, we also have found that the cytotoxicity of plumbagin in MCF-7 cells results from increased G2/M phase arrest with a reduction in cyclin B1.

The increased G2/M phase arrest ultimately increased apoptosis of MCF-7 cells, as indicated by the result of a significant increase of cleaved PARP level. Following the treatment of MCF-7 cell with plumbagin, we observed that significant increases in the Bax/Bcl-2 ratio and cytochrome c release, indicating that changes of these protein levels might contribute to the occurrence of mitochondria-related apoptotic cell death (Ahn et al., 2012; Hengartner, 2000; Wang et al., 2015). This

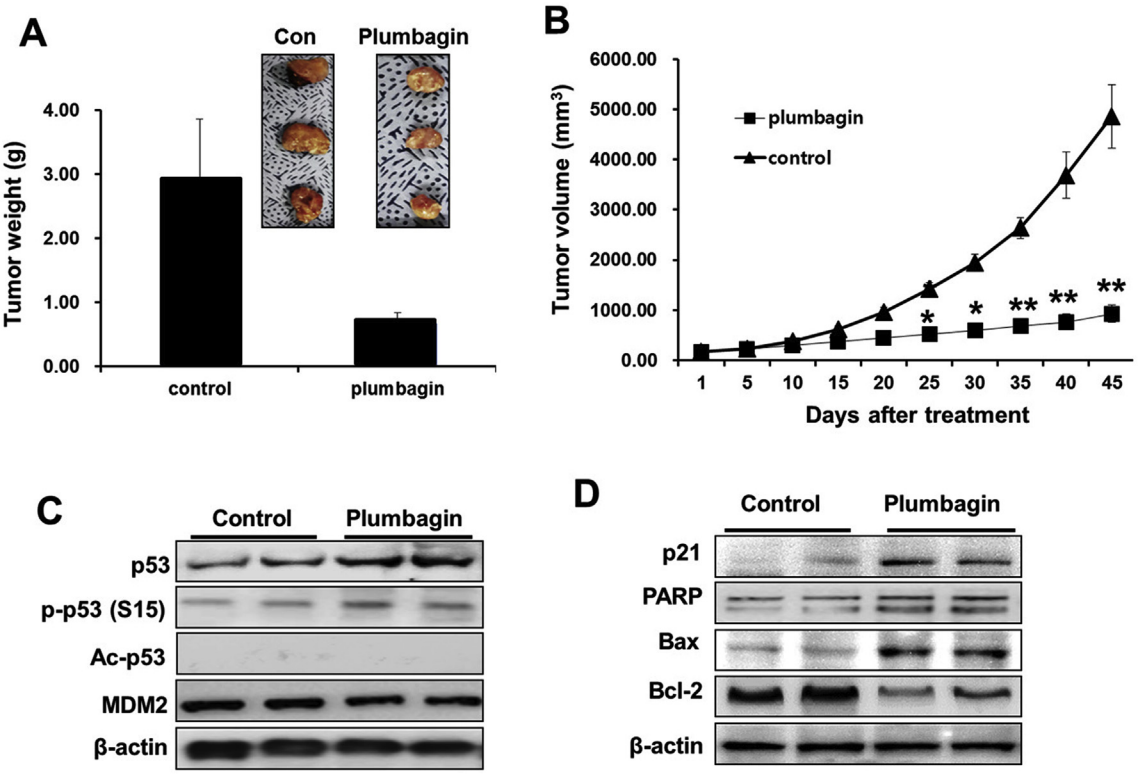

Fig. 6. *In vivo* xenograft model of MCF-7 confirms antitumor effect and cytotoxic mechanisms of plumbagin. Effects of plumbagin treatment on the growth of tumor-bearing nude mice inoculated with MCF-7 cells. Animals bearing pre-established tumors and control mice were each grouped randomly into 2 groups with 5 mice in each group. Then, i.p. injections of plumbagin (2 mg/kg) or vehicle were initiated after tumor volume reached above 150 mm^3. (A) Each bar represents the mean of tumor weight. The weight of each harvested tumor was measured and plotted. Mice from both groups were sacrificed at 45 days and tumors were isolated from the mice at the end of treatment. Photographs of representative tumors are shown. (B) During the 45-day treatment, tumor volumes were estimated using measurements taken from external calipers (millimeters cubed). The graph represents tumor size of control and plumbagin-treated mice. (C–D) Total protein was collected from two tumors per treated or untreated mouse and then western blot analysis was performed with antibodies against PARP, p21, Bax, Bcl-2, p53, phospho-p53, Ac-p53, MDM2, and β-actin (as a loading control). Each value in the graph represents the mean ± SD from five mice. *$p < 0.05$; **$p < 0.01$ were considered as significant.

is consistent with the results of previous research into the involvement of Bcl-2 family proteins in plumbagin-induced apoptosis in estrogen-positive cells, which showed that plumbagin induces apoptosis in HER2-overexpressing breast cancer cells occurred through the intrinsic pathway (Kawiak et al., 2017; Sagar et al., 2014). Our finding also showed a significant increase in early-stage apoptotic cell populations using flow cytometry analysis in MCF-7 cells. In particular, plumbagin-mediated apoptosis occurred at a low drug concentration that did not show any cytotoxicity in the MTT assay. Therefore, we suggested that the toxicity of plumbagin to normal cells might be minimal during the therapeutic use of plumbagin in patients with cancer.

In the present study, we suggested that plumbagin-induced apoptosis may be a result of intracellular ROS generation, which specifically contributes to anticancer activity in breast cancer cells with wild-type p53. Previous studies indicated that plumbagin have shown to induce cell death via ROS generation in many type of cancer cells (Lee et al., 2012; Srinivas et al., 2004; Wang et al., 2008; Xu and Lu, 2010). Therefore, we tried to further investigate the molecular mechanism of plumbagin on ROS generation in MCF-7 cells. Our results showed that plumbagin caused strong ROS generation in MCF-7 cells in a concentration-dependent manner. Additionally, plumbagin-mediated cell death was also significantly attenuated with NAC-pretreatment. Thus, we conclude that plumbagin-mediated cytotoxicity to cancer cells is closely associated with ROS generation. The proposed antitumor activity of plumbagin was further confirmed by *in vivo* findings of markedly reduced tumor weights and volumes in a mouse xenograft model. In the present study, plumbagin treatment significantly delayed the growth of MCF-7 xenograft tumors and increased p53 and p53 phosphorylation. Collectively, plumbagin exerted its growth suppressive activity in MCF-7 by inducing apoptotic-related proteins, which may provide an explanation for cancer cells apoptosis. Therefore, it is possible that apoptosis pathways are involved in the anticancer activity of plumbagin in MCF-7 ells.

5. Conclusion

Our results confirmed that plumbagin exhibits antitumor activity against human breast cancer cells. In addition, we provided further details elucidating the molecular mechanism underlying its function and demonstrated its efficacy using *in vivo* xenograft model. Therefore, plumbagin might act as a lead molecule for further development of drugs targeting p53-wild-type cancer cells. These finding also suggest that plumbagin from plant extracts can be used in clinical settings as a supplementary therapy for anticancer medicine.

Author contributions

Kim HS, Yoon S, and Kwak JH designed the experiments and drafted the manuscript. Kim IS, Ha KT, Choi WS, and Lee BM revised the manuscript. De U, Jeon Y, Ha S-Y, and Park YJ carried out isolation, western blotting and statistical analyses. De U, and Son JY performed the animal experiments.

Author disclosure statement

The authors declare that the research was conducted in the absence of any commercial or financial relationships that could be construed as a potential conflict of interest.

Acknowledgements

This work was supported by National Research Foundation of Korea grants funded by the Korean Government (NRF-2016R1A2B2011071, NRF-2016R1A4A1011189 and NRF-2017R1D1A1B03036571). We thank Ms. Hyerin Kwak for reading the manuscript.

Transparency document

Transparency document related to this article can be found online at https://doi.org/10.1016/j.fct.2018.11.040.

References

Ahn, M.Y., Kang, D.O., Na, Y.J., Yoon, S., Choi, W.S., Kang, K.W., Chung, H.Y., Jung, J.H., Min, doS., Kim, H.S., 2012. Histone deacetylase inhibitor, apicidin, inhibits human ovarian cancer cell migration via class II histone deacetylase 4 silencing. Cancer Lett. 325, 189–199. https://doi.org/10.1016/j.canlet.2012.06.017.

Aziz, M.H., Dreckschmidt, N.E., Verma, A.K., 2008. Plumbagin, a medicinal plant-derived naphthoquinone, is a novel inhibitor of the growth and invasion of hormone-refractory prostate cancer. Cancer Res. 68, 9024–9032. https://doi.org/10.1158/0008-5472.CAN-08-2494.

Bauer, U., Federle, W., 2009. The insect-trapping rim of Nepenthes pitchers. Plant Signal. Behav. 4, 1019–1023.

Buch, F., Rott, M., Rottloff, S., Paetz, C., Hilke, I., Raessler, M., Mithöfer, A., 2013. Secreted pitfall-trap fluid of carnivorous Nepenthes plants is unsuitable for microbial growth. Ann. Bot. 111, 375–383. https://doi.org/10.1093/aob/mcs287.

Cannon, J.R., Lojanapiwatna, V., Raston, C.L., Shinchai, W., White, A.H., 1980. The Quinones of *Nepenthes rafflesiana*. The crystal structure of 2,5-dihydroxy-3,8-dimethoxy-7-methylnaphtho-1,4-quinone (Nepenthone-E) and a synthesis of 2,5-dihydroxy-3-methoxy-7-methylnaphthp-1,4-quinone (Nepenthone-C). Aust. J. Chem. 33, 1073–1093.

Girardini, J.E., Walerych, D., Del Sal, G., 2014. Cooperation of p53 mutations with other oncogenic alterations in cancer. Subcell. Biochem. 85, 41–70. https://doi.org/10.1007/978-94-017-9211-0_3.

Gowda, R., Sharma, A., Robertson, G.P., 2017. Synergistic inhibitory effects of Celecoxib and Plumbagin on melanoma tumor growth. Cancer Lett. 385, 243–250. https://doi.org/10.1016/j.canlet.2016.10.016.

Hafeez, B.B., Zhong, W., Fischer, J.W., Mustafa, A., Shi, X., Meske, L., Hong, H., Cai, W., Havighurst, T., Kim, K., Verma, A.K., 2013. Plumbagin, a medicinal plant (*Plumbago zeylanica*)-derived 1,4-naphthoquinone, inhibits growth and metastasis of human prostate cancer PC-3M-luciferase cells in an orthotopic xenograft mouse model. Mol. Oncol. 7, 428–439. https://doi.org/10.1016/j.molonc.2012.12.001.

Hengartner, M.O., 2000. The biochemistry of apoptosis. Nature (Lond.) 407, 770–776.

Huxley, A., Griffiths, M., Levy, M., 1999. The New Royal Horticultureal Society Dictionary of Gardening. Macmillan Reference LTD, London, United Kingdom, pp. 307.

Inoue, K., Fry, E.A., 2016. Aberrant splicing of the DMP1-ARF-MDM2-p53 pathway in cancer. Int. J. Canc. 139, 33–41. https://doi.org/10.1002/ijc.30003.

Kawiak, A., Domachowska, A., Jaworska, A., Lojkowska, E., 2017. Plumbagin sensitizes breast cancer cells to tamoxifen-induced cell death through GRP78 inhibition and Bik upregulation. Sci. Rep. 7, 43781. https://doi.org/10.1038/srep43781.

Kim, T.H., Shin, Y.J., Won, A.J., Lee, B.M., Choi, W.S., Jung, J.H., Chung, H.Y., Kim, H.S., 2014. Resveratrol enhances chemosensitivity of doxorubicin in multidrug-resistant human breast cancer cells via increased cellular influx of doxorubicin. Biochim. Biophys. Acta 1840, 615–625. https://doi.org/10.1016/j.bbagen.2013.10.023.

Kim, T.H., Kim, H.S., Kang, Y.J., Yoon, S., Lee, J., Choi, W.S., Jung, J.H., Kim, H.S., 2015. Psammaplin A induces Sirtuin 1-dependent autophagic cell death in doxorubicin-resistant MCF-7/adr human breast cancer cells and xenografts. Biochim. Biophys. Acta 1850, 401–410. https://doi.org/10.1016/j.bbagen.2014.11.007.

Lee, J.H., Yeon, J.H., Kim, H., Roh, W., Chae, J., Park, H.O., Kim, D.M., 2012. The natural anticancer agent plumbagin induces potent cytotoxicity in MCF-7 human breast cancer cells by inhibiting a PI-5 kinase for ROS generation. PloS One 7, e45023 10.1371.

Manu, K.A., Shanmugam, M.K., Rajendran, P., Li, F., Ramachandran, L., Hay, H.S., Kannaiyan, R., Swamy, S.N., Vali, S., Kapoor, S., Ramesh, B., Bist, P., Koay, E.S., Lim, L.H., Ahn, K.S., Kumar, A.P., Sethi, G., 2011. Plumbagin inhibits invasion and migration of breast and gastric cancer cells by downregulating the expression of chemokine receptor CXCR4. Mol. Canc. 10, 107. https://doi.org/10.1186/1476-4598-10-107.

Mithöfer, A., 2011. Carnivorous pitcher plants: insights in an old topic. Phytochemistry 72, 1678–1682. https://doi.org/10.1016/j.phytochem.2010.11.024.

Nair, R.S., Kumar, J.M., Jose, J., Somasundaram, V., Hemalatha, S.K., Sengodan, S.K., Nadhan, R., Anilkumar, T.V., Srinivas, P., 2016. Increased sensitivity of BRCA defective triple negative breast tumors to plumbagin through induction of DNA double strand breaks (DSB). Sci. Rep. 6, 26631. https://doi.org/10.1038/srep26631.

Padhye, S., Dandawate, P., Yusufi, M., Ahmad, A., Sarkar, F.H., 2012. Perspectives on medicinal properties of plumbagin and its analogs. Med. Res. Rev. 32, 1131–1158. https://doi.org/10.1002/med.20235.

Pan, S.T., Qin, Y., Zhou, Z.W., He, Z.X., Zhang, X., Yang, T., Yang, Y.X., Wang, D., Qiu, J.X., Zhou, S.F., 2015. Plumbagin induces G2/M arrest, apoptosis, and autophagy via p38 MAPK- and PI3K/Akt/mTOR-mediated pathways in human tongue squamous cell carcinoma cells. Drug Des. Dev. Ther. 9, 1601–1626. https://doi.org/10.2147/DDDT.S76057.

Qiao, H., Wang, T.Y., Yu, Z.F., Han, X.G., Liu, X.Q., Wang, Y.G., Fan, Q.M., Qin, A., Tang, T.T., 2016. Structural simulation of adenosine phosphate via plumbagin and zoledronic acid competitively targets JNK/Erk to synergistically attenuate osteoclastogenesis in a breast cancer model. Cell Death Dis. 7https://doi.org/10.1038/cddis.2016.11. e2094.

Raj, G., Kurup, R., Hussain, A.A., Baby, S., 2011. Distribution of naphthoquinones, plumbagin, droserone, and 5-O-methyl droserone in chitin-induced and uninduced *Nepenthes khasiana*: molecular events in prey capture. J. Exp. Bot. 62, 5429–5436. https://doi.org/10.1093/jxb/err219.

Rischer, H., Hamm, A., Bringmann, G., 2002. *Nepenthes insignis* uses a C2-portion of the carbon skeleton of L-alanine acquired via its carnivorous organs, to build up the allelochemical plumbagin. Phytochemistry 59, 603–609.

Sagar, S., Esau, L., Moosa, B., Khashab, N.M., Bajic, V.B., Kaur, M., 2014. Cytotoxicity and apoptosis induced by a plumbagin derivative in estrogen positive MCF-7 breast cancer cells. Anti Cancer Agents Med. Chem. 14, 170–180.

Schlauer, J., Nerz, J., Richer, H., 2005. Carnivorous plant chemistry. Acta Bot. Gall. 152, 187–195.

Sinha, S., Pal, K., Elkhanany, A., Dutta, S., Cao, Y., Mondal, G., Iyer, S., Somasundaram, V., Couch, F.J., Shridhar, V., Bhattacharya, R., Mukhopadhyay, D., Srinivas, P., 2013. Plumbagin inhibits tumorigenesis and angiogenesis of ovarian cancer cells in vivo. Int. J. Canc. 132, 1201–1212. https://doi.org/10.1002/ijc.27724.

Srinivas, P., Gopinath, G., Banerji, A., Dinakar, A., Srinivas, G., 2004. Plumbagin induces reactive oxygen species, which mediate apoptosis in human cervical cancer cells. Mol. Carcinog. 40, 201–211.

Thasni, K.A., Ratheeshkumar, T., Rojini, G., Sivakumar, K.C., Nair, R.S., Srinivas, G., Banerji, A., Somasundaram, V., Srinivas, P., 2013. Structure activity relationship of plumbagin in BRCA1 related cancer cells. Mol. Carcinog. 52, 392–403. https://doi.org/10.1002/mc.21877.

Tian, L., Yin, D., Ren, Y., Gong, C., Chen, A., Guo, F.J., 2012. Plumbagin induces apoptosis via the p53 pathway and generation of reactive oxygen species in human osteosarcoma cells. Mol. Med. Rep. 5, 126–132. https://doi.org/10.3892/mmr.2011.624.

Wang, C.C., Chiang, Y.M., Sung, S.C., Hsu, Y.L., Chang, J.K., Kuo, P.L., 2008. Plumbagin induces cell cycle arrest and apoptosis through reactive oxygen species/c-Jun N-terminal kinase pathways in human melanoma A375.S2 cells. Cancer Lett. 259, 82–98.

Wang, J., Guo, W., Zhou, H., Luo, N., Nie, C., Zhao, X., Yuan, Z., Liu, X., Wei, Y., 2015. Mitochondrial p53 phosphorylation induces Bak-mediated and caspase-independent cell death. Oncotarget 6, 17192–17205. https://doi.org/10.18632/oncotarget.3780.

Wei, Y., Yang, Q., Zhang, Y., Zhao, T., Liu, X., Zhong, J., Ma, J., Chen, Y., Zhao, C., Li, J., 2017. Plumbagin restrains hepatocellular carcinoma angiogenesis by suppressing the migration and invasion of tumor-derived vascular endothelial cells. Oncotarget 8, 15230–15241. https://doi.org/10.18632/oncotarget.14774.

Xu, K.H., Lu, D.P., 2010. Plumbagin induces ROS-mediated apoptosis in human promyelocytic leukemia cells in vivo. Leuk. Res. 34, 658–665.

Zhang, X.Q., Yang, C.Y., Rao, X.F., Xiong, J.P., 2016. Plumbagin shows anti-cancer activity in human breast cancer cells by the upregulation of p53 and p21 and suppression of G1 cell cycle regulators. Eur. J. Gynaecol. Oncol. 37, 30–35.